ACADEMIC PRESS

Available online at www.sciencedirect.com

SCIENCE DIRECT®

Journal of Sound and Vibration 264 (2003) 851–872

JOURNAL OF SOUND AND VIBRATION

www.elsevier.com/locate/jsvi

Wave reflection and transmission in beams containing delamination and inhomogeneity

C.H. Wang*, L.R.F. Rose

Defence Science and Technology Organisation, 506 Lorimer Street, Fishermans Bend, Vic. 3207, Australia

Received 10 December 2001; accepted 5 August 2002

Abstract

This paper presents an analytical approach using higher order plate theories to determine wave reflections from and transmissions through a damaged region in a beam. The damaged region is either treated as two split beams or as an inhomogeneity. The reflection ratios and transmission ratios are found to depend strongly on the frequency of the incident flexural waves, as well as the size of the damage, which gives rise to strong stop/pass band behaviour. Using the spectral analysis method, the transient wave propagation in a beam with a part-through delamination is predicted and compared with experimental results, indicating a good agreement in the phases and amplitudes of both the reflected and transmitted waves.

1. Introduction

Structural health (damage) monitoring using embedded actuators and sensors has received significant attention recently as a promising means for improved asset maintenance and structural integrity management [1–3]. In this regard, quantitative detection of damage (such as corrosion of metallic materials and delamination in fibre reinforced composites), which is critical to the assessment of its impact to structural safety, remains a significant challenge, although recent efforts using Lamb waves have shown considerable promises [4–9]. Since most load-bearing composite structures are designed to tolerate 10–20 mm diameter delaminations [4,5], structural health monitoring techniques should ideally be able to reliably detect delamination damage less than this design limit.

*Corresponding author.
E-mail address: chun-hui.wang@dsto.defence.gov.au (C.H. Wang).

0022-460X/03/$ - see front matter
doi:10.1016/S0022-460X(02)01193-8

It is now recognized that the resonant frequencies of plates or shells are not very sensitive to small delaminations [10,11], even for modes up to orders of 20–30 [12]. The main reason for this lack of sensitivity of vibration response to local damage is because the resonant frequency depends strongly on the overall size of a component and its boundary supports. Consequently, a more sensitive approach would be to probe changes associated with localized damage directly, such as exploiting the influence of damages on the propagation of stress waves [3,13]. In this case, parameters of primary importance are the magnitudes and phases of the reflected and transmitted waves. For plate-like structures, the Rayleigh–Lamb (see e.g.,Ref. [14]) waves have been the method of choice in the majority of investigations [4–9]. Although the Rayleigh–Lamb solution is exact, it is rather unwieldy for characterizing the wave reflection from and transmission through a damage, due to the need to account for the mode conversions among an infinite number of wave modes. Even when the excitation frequency is below the cut-off frequency of the first order modes (i.e., there is only one propagating incident wave), the higher order modes, which are near-field waves, are crucial to the satisfaction of continuity conditions and equilibrium conditions at the edge of a damaged region.

An alternative approach would be to employ higher order plate theories [15] to characterize the flexural waves [16] and extensional waves [17]. The Mindlin flexural wave theory can be viewed as an extension of Timoshenko beam theory to plates. Compared to methods based on Rayleigh–Lamb waves, plate wave approach offers several important advantages [18,19]. For instance, it greatly simplifies the determination of the effect of a damage on the reflected and transmitted waves, as will be demonstrated later in this paper. Furthermore, the plate wave method allows the effects of material damping or energy dissipation on wave attenuation to be readily taken into account. Other advantages include the applicability to orthotropic materials, such as composite materials. More importantly, the plate wave method enables the boundary effects of finite size plates to be predicted [20], which is critical to the development of a viable structural health prognostic technique for complex structures. Doyle and Kamle [21] demonstrated the applicability of elementary beam theory in capturing the transient wave propagation in a beam subjected to low-energy impact.

Due to the importance of delamination damage in composites, which are often invisible to the naked eye, several studies have examined the influence of delamination, in the simple case of a beam containing through-width delamination, on the vibration and wave propagation behaviour of beams. Wang et al. [22], and Tracy and Pardoen [11] analyzed a split beam, with the split region being treated as two separate beams, using the elementary beam theory. Mujumdar and Suryanarayan [23] addressed one deficiency of the analysis by Wang et al. [22] in the case of asymmetric delamination by treating the split region as two coupled beams with identical transverse displacement, but still within the framework of elementary beam theory. Farris and Doyle [24] employed the Timoshenko beam theory to analyze the split beam problem, with the split region being treated as two separate beams. None of these analysis considered the influence of multiple reflection/transmission at the two ends of a delamination. In the context of noise/vibration isolation, Mace et al. [25] investigated the wave reflection/transmission in a three waveguide system, accounting for multiple reflections/transmissions at the junctions, but the analysis was limited to the elementary beam theory. A different approach, as first proposed by Kulkarni and Frederick [10], is to model the effect of delamination as a *reduced bending rigidity* over the delamination zone. The moment of inertia of the delaminated zone was taken to be the

sum of the moments of inertia of the delaminated layers [10]. This homogenization approach, which is most appropriate for the case of multiple delaminations induced by impact damages, is more readily extended to a two dimensional (2-D) analysis [18,19].

The purpose of this paper is to present an analytical method to determine the reflections from and transmissions through a delaminated region in a one-dimensional (1-D) beam which is modelled using the Timoshenko beam theory. Two different approaches, a homogenization approach and a micro-mechanics approach, will be developed, in which the delaminated region is either modelled, respectively, as an equivalent inhomogeneity or as two split beams (Fig. 1). This paper is structured as follows. Section 2 summarizes the equations and solutions according to Timoshenko beam theory and Kane–Mindlin's extensional plate theory. In Section 3 the reflection and transmission coefficients for a beam with a semi-infinite delamination and a bimaterial beam are determined, corresponding to the micro-mechanics approach and the

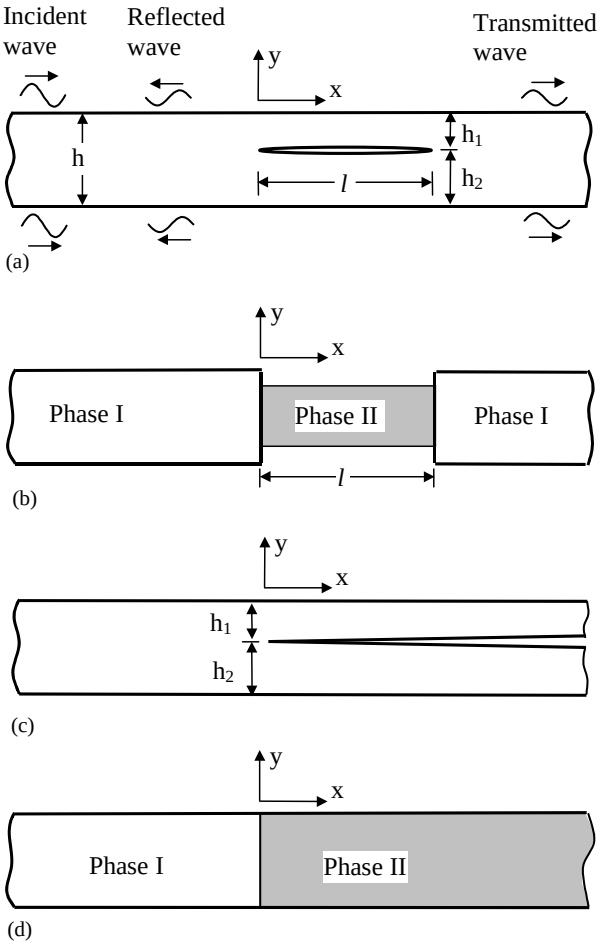

Fig. 1. Delamination in a beam: (a) delamination of finite length; (b) a beam containing an inhomogeneity; (c) a semi-infinite delamination; (c) a bimaterial system.

homogenization approach, respectively. These analyses are then extended in Section 4 to a damage zone of finite length, to account for multiple reflections and transmissions. Finally, a comparison is also made in Section 5 with experimental results of Diaz Valdes and Soutis [6] to demonstrate the capability of the analytical method.

2. Dispersion relationship for plate waves

2.1. Flexural waves

The equations of motion of Timoshenko beam theory are expressed in terms of the lateral displacement w and the angle of rotation θ [26,27],

$$\kappa^2 c_s^2 \left[\frac{\partial^2 w}{\partial x^2} - \frac{\partial \theta}{\partial x}\right] - \frac{\partial^2 w}{\partial t^2} = 0, \tag{1a}$$

$$c_0^2 \frac{\partial^2 \theta}{\partial x^2} + \kappa^2 \frac{c_s^2}{q^2}\left[\frac{\partial w}{\partial x} - \theta\right] - \frac{\partial^2 \theta}{\partial t^2} = 0, \tag{1b}$$

where κ denotes a shear correction factor and (referring to nomenclature for symbols)

$$c_0 = \sqrt{E'/\rho}, \quad c_s = \sqrt{G/\rho}, \quad q = \sqrt{I/A}, \quad \kappa = \pi/\sqrt{12}. \tag{2}$$

Dispersion relations can be obtained by substituting the following expressions into the Timoshenko equations:

$$w = w_0 e^{-i(kx-\omega t)}, \quad \theta = \theta_0 e^{-i(kx-\omega t)} \tag{3}$$

yielding eigenvectors (which give the relationship between w_0 and θ_0) and the following four eigenroots:

$$k_m = \pm \left[\frac{1}{2}\left(1 + \frac{c_0^2}{\kappa^2 c_s^2}\right) \pm \sqrt{\left(\frac{c_0}{q\omega}\right)^2 + \frac{1}{4}\left(1 - \frac{c_0^2}{\kappa^2 c_s^2}\right)^2}\right]^{1/2} \frac{\omega}{c_0} \quad (m = 1, 2, 3, 4) \tag{4}$$

Depending on the frequency, there are either only two propagating waves (one positive-going and one negative-going) plus two evanescent (near-field) waves or four propagating waves (two positive-going and two negative-going). The cut-off frequency for the second flexural mode, obtained by setting $k_2 = 0$, is

$$\omega_c = \kappa \frac{c_s}{q}. \tag{5}$$

In the case of a beam with a rectangular cross-section ($q = h/\sqrt{12}$), the Timoshenko beam theory correctly recovers the cut-off frequency given by the Rayleigh–Lamb solution $\omega_c = \pi c_s/h$ by setting $\kappa = \pi/\sqrt{12}$.

A general solution of the homogeneous equations (1a) and (1b) is given by

$$\theta(x, t) = \sum_{m=1}^{4} a_m e^{-ik_m x} e^{i\omega t}, \tag{6}$$

$$w(x,t) = \sum_{m=1}^{4} a_m F_m e^{-ik_m x} e^{i\omega t}, \tag{7}$$

where the amplitude ratios are given by the eigenvector,

$$F_m = \frac{ik_m}{k_m^2 - (\omega/\kappa c_s)^2} \quad (m = 1,2,3,4). \tag{8}$$

Phase velocities and group velocities are given by $c_p = \omega/k$ and $c_g = d\omega/dk$. It is can be seen from Eq. (4) that both velocities depend parametrically on only two non-dimensional variables, q/λ and $c_0/\kappa c_s$, where λ denotes the wavelength.

The dispersion curves based on Eq. (4) are shown in Fig. 2 together with the exact solution of the Rayleigh–Lamb theory (see e.g., Ref. [14]). It is clear that the Timoshenko beam theory is accurate for the first flexural mode at any frequency, and is accurate for the second mode for $\omega \leqslant 1.3\omega_c$ approximately. By contrast, the Euler beam theory is accurate only up to about 5% of the cut-off frequency $\omega \leqslant 0.05\omega_c$.

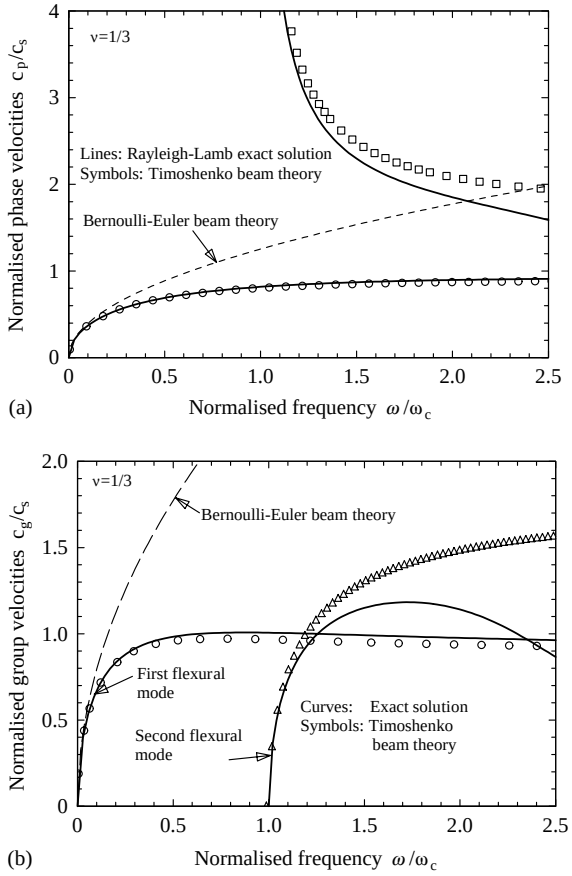

Fig. 2. Flexural waves in a homogeneous beam: (a) phase velocity and (b) group velocity.

2.2. Extensional waves

The higher order plate theory by Kane and Mindlin [17] can be viewed as the equivalent of Timoshenko beam theory for extensional waves: it is a fourth order plate theory and predicts two extensional waves. The wave numbers can be expressed as follows, setting the shear correction factor $\kappa = \pi/\sqrt{12}$,

$$k_m = \pm\frac{\omega}{c_s}\left[\frac{3-4\nu}{4-4\nu} - \frac{\pi^2}{1-\nu}\frac{c_s^2}{\omega^2 h^2} \pm \sqrt{\left(\frac{3-4\nu}{4-4\nu} - \frac{\pi^2}{1-\nu}\frac{c_s^2}{\omega^2 h^2}\right)^2 - \frac{c_s^2}{c_\ell^2} + \frac{\pi^2 c_s^2}{\omega^2 h^2}}\right]^{1/2}$$
$$(m = 1, 2, 3, 4), \tag{9}$$

where $c_\ell (= c_s\sqrt{2(1-\nu)/(1-2\nu)})$ denotes the longitudinal wave speed. The cut-off frequency for the second extensional mode is

$$\omega_{ce} = \pi c_\ell / h \tag{10}$$

which is equal to twice the cut-off frequency of flexural wave ω_c in Eq. (5) in the case of $\nu = 1/3$. Results of the phase and group velocities for the extensional waves are shown in Fig. 3, together

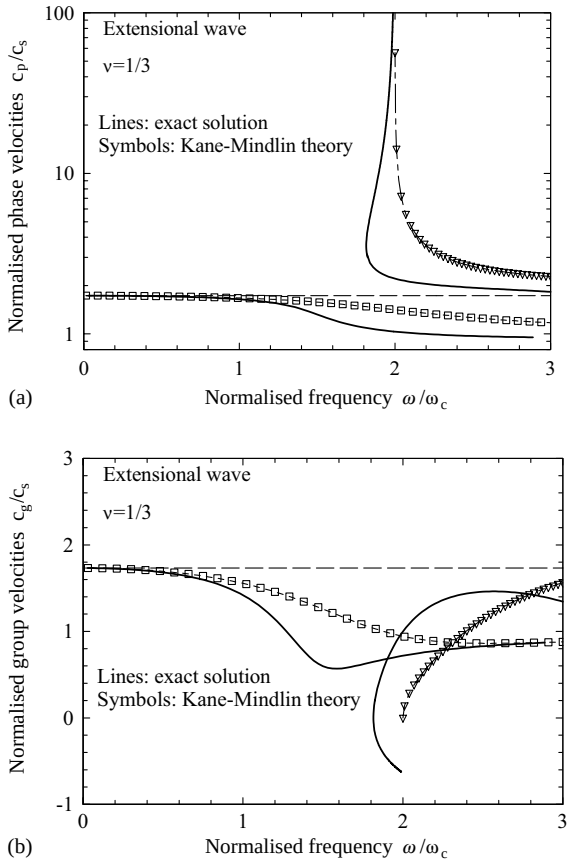

Fig. 3. Extensional waves in a homogeneous beam: (a) phase velocity and (b) group velocity.

with the exact solutions by Rayleigh–Lamb theory. In the limit of infinite frequency ($\omega \to \infty$), the phase velocities of the first and second extensional modes asymptote to c_s and $2c_s$, respectively. Therefore, the Kane–Mindlin theory correctly recovers the wave speeds of the first extensional mode at both the limits of zero frequency and infinite frequency, thus providing an improved solution over the elementary rod theory. However, for frequencies above the cut-off frequency of the second flexural wave (or half the cut-off frequency of the second extensional mode) the accuracy of the Kane–Mindlin theory drops off quite considerably [26]. These results indicate that, as compared to the elementary beam bending theory, the elementary rod theory seems to remain accurate up to the cut-off frequency ω_c of the second flexural wave. Improvement can be achieved by adding a third mode [27]. However, the additional degrees of freedom associated with the three-mode theory render applications to structural analysis significantly more complicated. Consequently, the simple rod theory will be employed in the present analysis.

3. Bimaterial and semi-infinite split beam

3.1. Homogenization approach

Consider a bimaterial beam shown in Fig. 1(d) with the positive-going incident waves given by

$$\theta_i(x,t) = [a\mathrm{e}^{-\mathrm{i}k_1 x} + b\mathrm{e}^{-\mathrm{i}k_2 x}]\mathrm{e}^{\mathrm{i}\omega t}, \tag{11}$$

$$w_i(x,t) = [F_1 a\mathrm{e}^{-\mathrm{i}k_1 x} + F_2 b\mathrm{e}^{-\mathrm{i}k_2 x}]\mathrm{e}^{\mathrm{i}\omega t}. \tag{12}$$

Since the second mode is a near-field (or evanescent) wave when the frequency is below the cut-off frequency, i.e., $\omega < \omega_c$, the magnitude b of the second mode should be taken to be zero when the excitation is located at $x \to -\infty$. While the evanescent wave can therefore be ignored in characterizing the incident wave, it must be retained when determining the reflection and transmission coefficients [28]. The total displacement of the beam in the left-hand region $x \leqslant 0$ is given by the sum of the incident and reflected waves,

$$\theta_-(x,t) = [a\mathrm{e}^{-\mathrm{i}k_1 x} + b\mathrm{e}^{-\mathrm{i}k_2 x} + a_r\mathrm{e}^{\mathrm{i}k_1 x} + b_r\mathrm{e}^{\mathrm{i}k_2 x}]\mathrm{e}^{\mathrm{i}\omega t}, \tag{13}$$

$$w_-(x,t) = [F_1 a\mathrm{e}^{-\mathrm{i}k_1 x} + F_2 b\mathrm{e}^{-\mathrm{i}k_2 x} - F_1 a_r\mathrm{e}^{\mathrm{i}k_1 x} - F_2 b_r\mathrm{e}^{\mathrm{i}k_2 x}]\mathrm{e}^{\mathrm{i}\omega t}. \tag{14}$$

In the right-hand region $x \geqslant 0$, which represents a damaged material with different material and geometrical properties from the left-hand region, there are two transmitted flexural waves, with one being possibly a near-field wave. The displacement of the beam in the region $x \geqslant 0$ is thus given by

$$\theta_+(x,t) = [a_t\mathrm{e}^{-\mathrm{i}k_1^* x} + b_t\mathrm{e}^{-\mathrm{i}k_2^* x}]\mathrm{e}^{\mathrm{i}\omega t}, \tag{15}$$

$$w_+(x,t) = [F_1^* a_t\mathrm{e}^{-\mathrm{i}k_1^* x} + F_2^* b_t\mathrm{e}^{-\mathrm{i}k_2^* x}]\mathrm{e}^{\mathrm{i}\omega t}, \tag{16}$$

where

$$k_1^* = \left[\frac{1}{2}\left(\left(\frac{c_0^*}{\kappa c_s^*}\right)^2+1\right)+\sqrt{\left(\frac{c_0^*}{q^*\omega}\right)^2+\frac{1}{4}\left(\left(\frac{c_0^*}{\kappa c_s^*}\right)^2-1\right)^2}\right]^{1/2}\frac{\omega}{c_0^*}, \tag{17a}$$

$$k_2^* = \frac{|\omega-\kappa c_s^*/q^*|}{\omega-\kappa c_s^*/q^*}\left[\frac{1}{2}\left(\left(\frac{c_0^*}{\kappa c_s^*}\right)^2+1\right)-\sqrt{\left(\frac{c_0^*}{q^*\omega}\right)^2+\frac{1}{4}\left(\left(\frac{c_0^*}{\kappa c_s^*}\right)^2-1\right)^2}\right]^{1/2}\frac{\omega}{c_0^*}, \tag{17b}$$

$$F_m^* = \frac{\mathrm{i}k_m^*}{(k_m^*)^2-(\omega/\kappa c_s^*)^2} \tag{18}$$

with

$$c_0^* = \sqrt{E^*/\rho^*(1-(\nu^*)^2)}, \quad c_s^* = \sqrt{G^*/\rho^*}, \quad q^* = \sqrt{I^*/A^*}. \tag{19}$$

Here the superscript "$*$" is employed to distinguish parameters pertaining to the damaged region.

Since the beam is continuous at $x=0$, explicit expressions for the four unknowns (a_r, a_r, a_t, b_t) can be readily determined from the continuity conditions:

$$\theta_- = \theta_+, \quad w_- = w_+, \quad M_- = M_+, \quad V_- = V_+ \quad (\text{at } x=0), \tag{20}$$

where the bending moment and shear force are given by

$$M = E'I\frac{\partial\theta}{\partial x}, \; V = E'I\left[-\frac{\partial^2\theta}{\partial x^2}+\frac{1}{c_0^2}\frac{\partial^2\theta}{\partial t^2}\right] \tag{21}$$

The amplitudes of the reflected and transmitted waves are related to those of the incident wave via the following relationship:

$$\begin{Bmatrix} a_r \\ b_r \end{Bmatrix} = \begin{bmatrix} r_{11} & r_{12} \\ r_{21} & r_{22} \end{bmatrix}\begin{Bmatrix} a \\ b \end{Bmatrix}, \tag{22}$$

$$\begin{Bmatrix} a_t \\ b_t \end{Bmatrix} = \begin{bmatrix} t_{11} & t_{12} \\ t_{21} & t_{22} \end{bmatrix}\begin{Bmatrix} a \\ b \end{Bmatrix}, \tag{23}$$

where $[r]$ and $[t]$ denote the reflection matrix and the transmission matrix. The algebraic expressions for the amplitudes of the reflected and transmitted waves are rather lengthy, so will be omitted for the sake of brevity. Numerical values are shown in Fig. 4(a) and (b) for the reflection ratios and the transmission ratios for a special case of $I^* = I/4$, $A^* = A$ (leading to $q^* = q/2$), $E^* = E$, and $\rho^* = \rho$, which can be considered to represent a beam with a symmetric delamination. The cut-off frequency of the second flexural wave in damaged region is twice the cut-off frequency for the undamaged region for this case, and thus the damaged region has one propagating wave and one evanescent wave, provided that the incident wave is flexural only.

The fact that the off-diagonal terms in the reflection and transmission matrices (r_{12},r_{21},t_{12},t_{21}) are non-zero suggests that there is a significant level of mode conversion occurring at the junction. It is also clear that magnitudes of the near-field waves are comparable to or even greater than

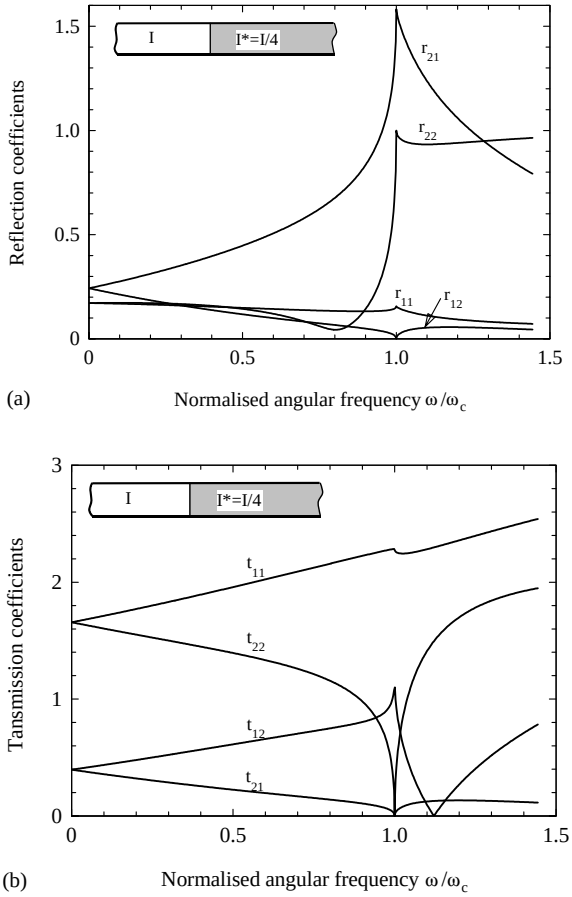

Fig. 4. Reflection and transmission at the boundary of an inhomogeneity: (a) reflection coefficients and (b) transmission coefficients.

those of the propagating waves, even for frequencies below ω_c, indicating the importance of accounting for the effect of mode conversion. It is worth noting that in the limit of $\omega \to 0$, the present results recover those according to elementary beam theory [28–30].

3.2. Micro-mechanics approach

Consider the case of a semi-infinite split beam as shown in Fig. 1(c). Using the Euler beam theory, Wang et al. [22] analyzed this problem with the split region being modelled as two separate beams, which led to overlapping between the two separated beams in the case of off-mid-plane (asymmetric) delamination. To address this problem, Mujumdar and Suryanarayan [23] presented an analysis in which the two split beams in the delaminated region were constrained to have identical transverse displacement, while free to slide over each other in the longitudinal direction. Again, this latter attempt was also restricted to the Euler beam theory, and hence the results are

limited to frequencies $\omega \ll \omega_c$. To extend the analysis to higher frequencies, Farris and Doyle [24] employed the Timoshenko beam theory, but the split region was modelled as two separate beams, which would lead to physically unrealistic overlapping between the two split beams in the case of asymmetric delamination. In the analysis presented here, the constrained beam approach of Mujumdar and Suryanarayan [23] is extended to analyze two coupled Timoshenko beams.

As in Section 3.1, the flexural waves (incident and reflected waves) in the region $x \leqslant 0$ are given by,

$$\theta_-(x,t) = [a e^{-ik_1 x} + b e^{-ik_2 x} + a_r e^{ik_1 x} + b_r e^{ik_2 x}] e^{i\omega t}, \tag{24}$$

$$w_-(x,t) = [F_1 a e^{-ik_1 x} + F_2 b e^{-ik_2 x} - F_1 a_r e^{ik_1 x} - F_2 b_r e^{ik_2 x}] e^{i\omega t}, \tag{25}$$

However, due to asymmetric delamination, a longitudinal wave is also reflected from and transmitted into the split beam region. The negative-going reflected longitudinal wave in the region ($x \leqslant 0$) can be expressed as

$$u_-(x,t) = g e^{ik_\ell x} e^{i\omega t}, \tag{26}$$

where $k_\ell = \omega/c_0$.

Denoting the contact pressure between the two split beams as $p(x)$, as shown in Fig. 5, with the identical displacement constraint, i.e., $\bar{w} = \bar{\bar{w}} \equiv \hat{w}$, the following governing equations can be derived:

$$\kappa^2 G \bar{A} \left[\frac{\partial^2 \hat{w}}{\partial x^2} - \frac{\partial \bar{\theta}}{\partial x} \right] = \rho \bar{A} \frac{\partial^2 \hat{w}}{\partial t^2} + p, \tag{27a}$$

$$E' \bar{I} \frac{\partial^2 \bar{\theta}}{\partial x^2} + \kappa^2 G \bar{A} \left[\frac{\partial \hat{w}}{\partial x} - \bar{\theta} \right] = \rho \bar{I} \frac{\partial^2 \bar{\theta}}{\partial t^2} \tag{27b}$$

for the upper split beam, and

$$\kappa^2 G \bar{\bar{A}} \left[\frac{\partial^2 \hat{w}}{\partial x^2} - \frac{\partial \bar{\bar{\theta}}}{\partial x} \right] = \rho \bar{\bar{A}} \frac{\partial^2 \hat{w}}{\partial t^2} - p, \tag{28a}$$

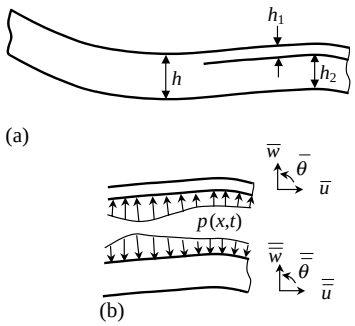

Fig. 5. Constrained split beam; (a) deformation in the beam with a split and (b) contact pressure between the split beams.

$$E'\,\bar{\bar{I}}\frac{\partial^2\bar{\bar{\theta}}}{\partial x^2}+\kappa^2 G\bar{\bar{A}}\left[\frac{\partial\hat{w}}{\partial x}-\bar{\bar{\theta}}\right]=\rho\,\bar{\bar{I}}\frac{\partial^2\bar{\bar{\theta}}}{\partial t^2} \tag{28b}$$

for the lower split beam.

The contact pressure p can be eliminated by adding Eqs. (27a) and (28a), noting $\bar{A}+\bar{\bar{A}}=A$, to obtain

$$\kappa^2 G\left[A\frac{\partial^2\hat{w}}{\partial x^2}-\bar{A}\frac{\partial\bar{\theta}}{\partial x}-\bar{\bar{A}}\frac{\partial\bar{\bar{\theta}}}{\partial x}\right]=\rho\,A\frac{\partial^2\hat{w}}{\partial t^2} \tag{29}$$

Dispersion relations can now be determined by substituting the following expressions into Eqs. (29), (27b) and (28b),

$$\bar{\theta}=\bar{\theta}_0 e^{-i(\hat{k}x-\omega t)},\quad \bar{\bar{\theta}}=\bar{\bar{\theta}}_0 e^{-i(\hat{k}x-\omega t)},\quad \hat{w}=\hat{w}_0 e^{-i(\hat{k}x-\omega t)}, \tag{30}$$

where the magnitudes $(\bar{\theta}_0,\bar{\bar{\theta}}_0,\hat{w}_0)$ and the wave number k are given by the following equation:

$$\begin{bmatrix}(\rho\omega^2-\kappa^2 G\hat{k}^2)A & i\kappa^2 G\bar{A}\hat{k} & i\kappa^2 G\bar{\bar{A}}\hat{k}\\ i\kappa^2 G\bar{A}\hat{k} & E'\bar{I}\hat{k}^2+\kappa^2 G\bar{A}-\rho\bar{I}\omega^2 & 0\\ i\kappa^2 G\bar{\bar{A}}\hat{k} & 0 & E'\bar{\bar{I}}\hat{k}^2+\kappa^2 G\bar{\bar{A}}-\rho\bar{\bar{I}}\omega^2\end{bmatrix}\begin{Bmatrix}\hat{w}_0\\ \bar{\theta}_0\\ \bar{\bar{\theta}}_0\end{Bmatrix}=0. \tag{31}$$

The resulting characteristic equation is bicubic, and has three roots, giving rise to three modes of flexural wave. The positive-going waves in the split beams can be described as

$$\bar{\theta}=a_t e^{-i(\hat{k}_1 x-\omega t)}+b_t e^{-i(\hat{k}_2 x-\omega t)}+c_t e^{-i(\hat{k}_3 x-\omega t)}, \tag{32}$$

$$\bar{\bar{\theta}}=\Gamma_1 a_t e^{-i(\hat{k}_1 x-\omega t)}+\Gamma_2 b_t e^{-i(\hat{k}_2 x-\omega t)}+\Gamma_3 c_t e^{-i(\hat{k}_3 x-\omega t)}, \tag{33}$$

$$\hat{w}=\Phi_1 a_t e^{-i(\hat{k}_1 x-\omega t)}+\Phi_2 b_t e^{-i(\hat{k}_2 x-\omega t)}+\Phi_3 c_t e^{-i(\hat{k}_3 x-\omega t)}, \tag{34}$$

where the ratios Γ_i and Φ_i $(i=1,2,3)$ can be determined from Eq. (31). The longitudinal waves in the two split beams are given by

$$\bar{u}(x,t)=\bar{g}e^{-ik_\ell x}e^{i\omega t}, \tag{35}$$

$$\bar{\bar{u}}(x,t)=\bar{\bar{g}}e^{-ik_\ell x}e^{i\omega t}, \tag{36}$$

From the following continuity and equilibrium conditions at $x=0$ the eight unknowns (g, $\bar{g}$, $\bar{\bar{g}}$, a_r, b_r, a_t, b_t, c_t) can be determined:

$$\begin{gathered}\theta_-=\bar{\theta},\quad \theta_-=\bar{\bar{\theta}},\quad w_-=\hat{w},\quad \bar{u}=u_--\theta_-\frac{h_1}{2},\quad \bar{\bar{u}}=u_-+\theta_-\frac{h_2}{2}\\ T_-=\bar{T}+\bar{\bar{T}},\quad M_-=\bar{M}+\bar{\bar{M}}-\bar{T}\frac{h_1}{2}+\bar{\bar{T}}\frac{h_2}{2},\quad V_-=\bar{V}+\bar{\bar{V}}\quad (x=0),\end{gathered} \tag{37}$$

where the longitudinal forces are given by

$$T_-=E'A\frac{\partial u_-}{\partial x},\quad \bar{T}=E'\bar{A}\frac{\partial\bar{u}}{\partial x},\quad \bar{\bar{T}}=E'\bar{\bar{A}}\frac{\partial\bar{\bar{u}}}{\partial x}. \tag{38}$$

It is also clear that the contact pressure p, which can be determined from Eq. (27a), exhibits a sinusoidal distribution along the beam length. Therefore the contact pressure may become negative at some locations along the beam, which indicates possible separation of the two split beams. A rigorous analysis would need to deal with the mixed boundary conditions (zero displacement over some portions of the beam and zero contact pressure over the remaining beam) between the two split beams. This will not be further pursued here.

In the case of symmetric delamination ($h_1 = h_2 = h/2$), it turns out that $\bar{\theta} \equiv \bar{\bar{\theta}}$ and $p \equiv 0$. Consequently, the characteristic equation (31) degenerates to that for a single split beam. In this case, there are only five unknowns ($\bar{g}$, a_r, b_r, a_t, b_t). The results of the reflection ratios and the transmission ratios versus the frequency of the incident flexural waves are shown in Fig. 6. A comparison with the results shown in Fig. 4 suggests that in the limit $\omega \to 0$ the homogenization method and the micro-mechanics method yield identical solutions. However, as the frequency increases, the two solutions start to deviate from each other.

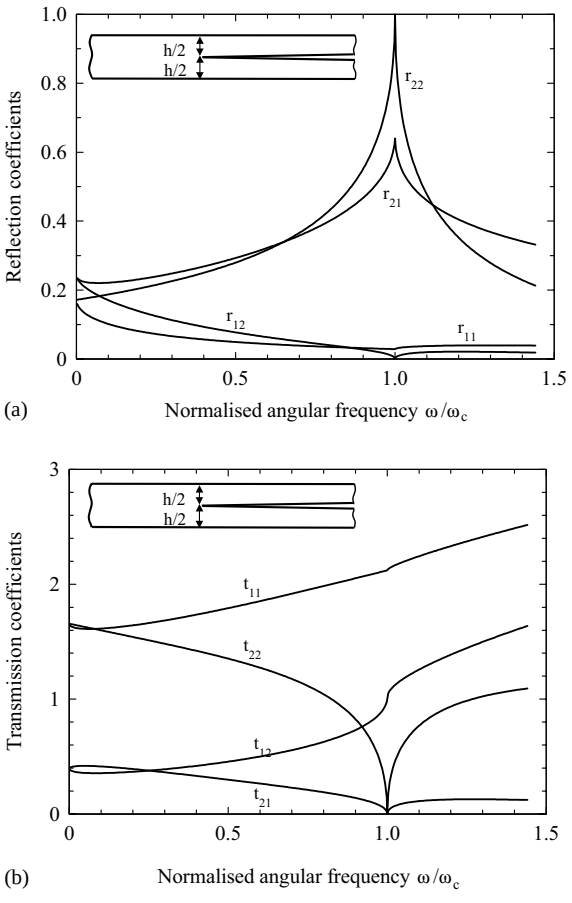

Fig. 6. Reflection and transmission in a symmetric split beam: (a) reflection coefficients and (b) transmission coefficients.

3.3. Power reflection and transmission

The power carried by a propagating wave in a Timoshenko beam can be determined by considering the total work done by internal forces (shear force and bending moment) across a section [30]. Referring to Fig. 7 for a section across the vibrating beam, the shear force (V) is in the same direction as the velocity ($\partial w/\partial t$), whereas the bending moment works against the rate of rotation ($\partial\theta/\partial t$). Therefore, the total average rate of working per unit time, or the power transmitted across the section, is

$$P = \frac{1}{T}\int_0^T \left[V\frac{\partial w}{\partial t} - M\frac{\partial \theta}{\partial t}\right] dt, \tag{39}$$

where T denotes the period of the propagating wave. Substituting the real parts of the incident and the reflected waves given by Eqs. (13) and (14), powers of the incident and the reflected waves can be expressed as

$$P_i = \left(\rho A|F_1|^2\frac{\omega^3}{k_1} + EI\omega k_1\right)\frac{|a|^2}{2} + \mathrm{H}(\omega-\omega_c)\left(\rho A|F_2|^2\frac{\omega^3}{k_2} + EI\omega k_2\right)\frac{|b|^2}{2}, \tag{40}$$

$$P_r = \left(\rho A|F_1|^2\frac{\omega^3}{k_1} + EI\omega k_1\right)\frac{|a_r|^2}{2} + \mathrm{H}(\omega-\omega_c)\left(\rho A|F_2|^2\frac{\omega^3}{k_2} + EI\omega k_2\right)\frac{|b_r|^2}{2}, \tag{41}$$

where the Heaviside function H is used to signify that the second wave carries energy only when the frequency is above its cut-off frequency. It can be shown that in the limit of $\omega\to 0$ (leading to $|F_1|\to 1/k_1$), the above expressions reduce to the solution by Mead [30] for the case of elementary beam theory.

Since the evanescent waves (the second incident and reflected waves when $\omega<\omega_c$, and the second transmitted wave when $\omega<\omega_c^*$) do not propagate energy along the beam, nor do they dissipate energy, the sum of the reflected energy and the transmitted energy is equal to the incident energy. This has also been confirmed by the numerical results discussed below. Therefore the transmitted energy can be readily determined from $P_t = P_i - P_r$. Fig. 8 shows the ratio of the reflected energy to the incident energy (P_r/P_i). It is seen that the reflected energy initially decreases with the frequency, then increases to reach a maximum at a frequency ten per cent above the cut-off frequency of second mode. For the inhomogeneous beam configuration, the reflected power shows only a mild decrease with frequency. However, for the case of split beam, the frequency has

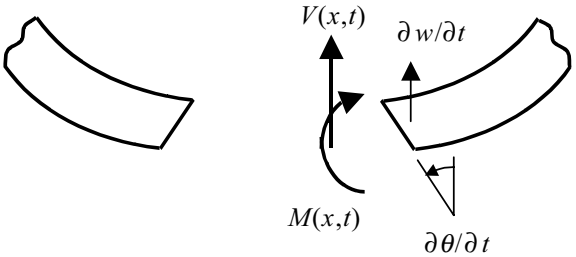

Fig. 7. Energy propagation by flexural wave in Timoshenko beam.

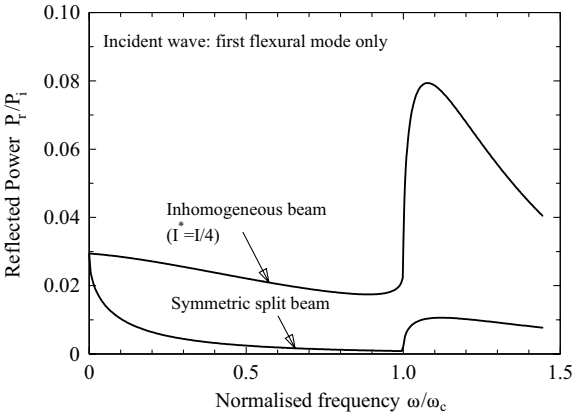

Fig. 8. Comparison of the power reflected at an interface.

a very strong influence on the reflected power, especially in the low-frequency limit. It is interesting to note that in the limit of zero frequency, i.e., $\omega \to 0$, both solutions converge to the solution of elementary beam theory [28,30]. The results also suggest that the split beam configuration exhibits a lower reflective index than the equivalent inhomogeneous configuration, primarily due to the mode conversion of flexural waves to longitudinal waves in the split beams.

4. Beam containing a finite size damage or symmetric delamination

4.1. Homogenization approach

Consider a beam containing an inhomogeneity of length l, as shown in Fig. 1(b). It is now necessary to account for multiple reflections and transmissions at both ends $x = 0$ and l. Consequently, a finite size damage will give rise to an infinite number of components, whose relative phases are determined by the total "round-trip" distance $2l$ traversed by these wave components, similar to wave propagation in structural inserts [25,29]. This sum of the infinite number of reflections will be determined below using the standing wave method.

In the region $x<0$ the incident and reflected flexural waves are given by

$$\theta_-(x,t) = [a\mathrm{e}^{-\mathrm{i}k_1 x} + b\mathrm{e}^{-\mathrm{i}k_2 x} + a_r\mathrm{e}^{\mathrm{i}k_1 x} + b_r\mathrm{e}^{\mathrm{i}k_2 x}]\mathrm{e}^{\mathrm{i}\omega t}, \tag{42}$$

$$w_-(x,t) = [aF_1\mathrm{e}^{-\mathrm{i}k_1 x} + bF_2\mathrm{e}^{-\mathrm{i}k_2 x} - a_rF_1\mathrm{e}^{\mathrm{i}k_1 x} - b_rF_2\mathrm{e}^{\mathrm{i}k_2 x}]\mathrm{e}^{\mathrm{i}\omega t} \tag{43}$$

except that the reflected waves (terms pertaining to a_r and b_r) comprise the superposition of multiple reflections at $x = 0$ and l, which will be determined from the continuity and equilibrium conditions at the two junctions.

In the damaged region $0<x<l$, there are two positive-going waves and two negative-going waves, resulting from the multiple reflections and transmissions at the two boundaries $x = 0$ and l.

The deformation is given by

$$\theta^*(x,t) = \sum_{m=1}^{4} a_m^* e^{-ik_m^* x} e^{i\omega t}, \tag{44}$$

$$w^*(x,t) = \sum_{m=1}^{4} F_m^* \, a_m^* \, e^{-ik_m^* x} \, e^{i\omega t}, \tag{45}$$

where k_m^* and F_m^* are given by Eqs. (18) and (17).

In the third region $x > l$, there are only two positive-going waves as given below:

$$\theta_L(x,t) = [a_t e^{-ik_1 x} + b_t e^{-ik_2 x}] e^{i\omega t}, \tag{46}$$

$$w_L(x,t) = [a_t F_1 e^{-ik_1 x} + b_t F_2 e^{-ik_2 x}] e^{i\omega t} \tag{47}$$

Therefore, the reflection from and transmission across a finite size inhomogeneity are characterized by eight unknown coefficients $(a_r, b_r, a_1^*, a_2^*, a_3^*, a_4^*, a_t, b_t)$, which can be determined from the following continuity and equilibrium conditions:

$$\theta_- = \theta^*, \quad w_- = w^*, \quad M_- = M^*, \quad V_- = V^* \quad (\text{at } x = 0), \tag{48a}$$

$$\theta^* = \theta_L, \quad w^* = w_L, \quad M^* = M_L, \quad V^* = V_L \quad (\text{at } x = l) \tag{48b}$$

Results for a special case of $I^* = I/4$ ($A^* = A$, $E^* = E$, $\rho^* = \rho$) are shown in Fig. 9, where the reflection and transmission coefficients are defined by Eqs. (22 and 23).

It is clear in Fig. 9 that the reflection ratio r_{11} oscillates between zero and maximum values that are dependent on the frequency as well as the bending stiffness of the inhomogeneity relative to that of the undamaged beam. This varying reflection ratio suggests that optimal frequencies exist for maximum reflection (minimum transmission) and zero reflection. Consequently, if the reflection response is to be used for the detection of inhomogeneities, the frequency of the incident wave may strongly affect the sensitivities. Furthermore, the reflection and transmission ratios depend on two variables: the normalized frequency and the ratio of damage size to beam thickness. At the low-frequency limit, however, the present results confirm that the reflection and transmission ratios depend on only one non-dimensional parameter $k_1 l$ [25,29].

4.2. Micro-mechanics approach to symmetric delamination

In the case when the main damage is due to a single delamination, a better approach is to model the delaminated region as consisting of split beams. In the following, attention is focused on the special case of symmetric delamination, whereas the analysis method is readily applicable to the asymmetric delamination using either the uncoupled beam or constrained beam approach outlined in Section 3.

Referring to Fig. 1(a), the flexural wave in the region $x \leqslant 0$ incident and reflected flexural waves are given by

$$\theta_-(x,t) = [a e^{-ik_1 x} + b e^{-ik_2 x} + a_r e^{ik_1 x} + b_r e^{ik_2 x}] e^{i\omega t}, \tag{49}$$

$$w_-(x,t) = [F_1 a e^{-ik_1 x} + F_2 b e^{-ik_2 x} - a_r F_1 e^{ik_1 x} - b_r F_2 e^{ik_2 x}] \; e^{i\omega t}. \tag{50}$$

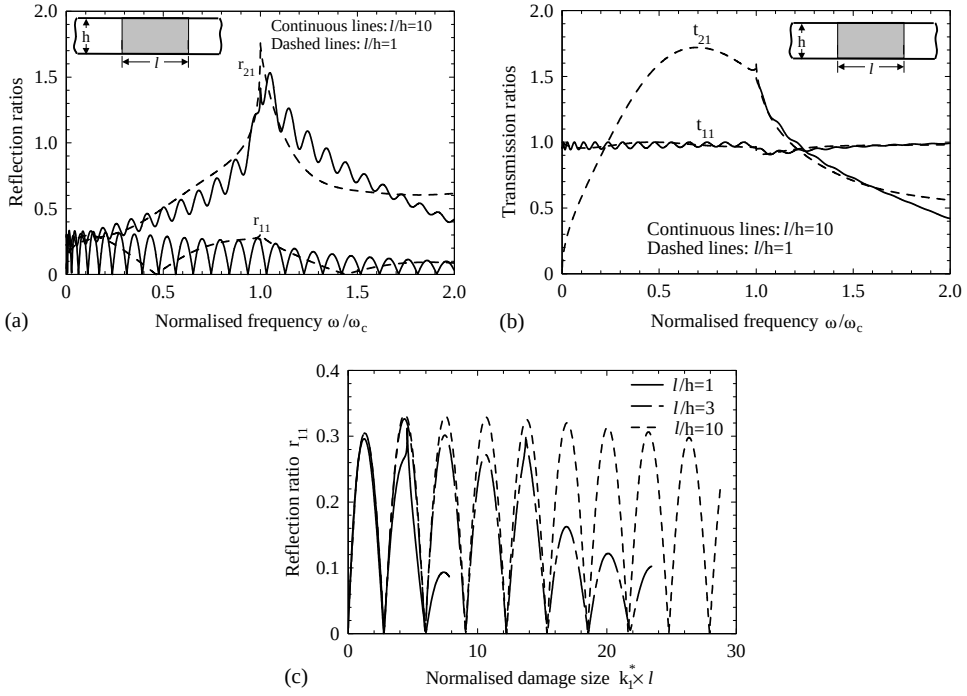

Fig. 9. Influence of a finite size inhomogeneity on wave reflection and transmission; (a) reflection coefficients, (b) transmission coefficients, and (c) reflection coefficient r_{11} versus normalized damage size.

For the delaminated region $(0<x<l)$, the waves in the two split beams are identical,

$$\bar{u}(x,t) = [\bar{g}e^{-i\bar{k}_\ell x} + \bar{h}e^{i\bar{k}_\ell x}]\, e^{i\omega t}, \tag{51}$$

$$\bar{\theta}(x,t) = [\bar{a}e^{-i\bar{k}_1 x} + \bar{b}e^{-i\bar{k}_2 x} + \bar{c}e^{i\bar{k}_1 x} + \bar{d}e^{i\bar{k}_2 x}]\, e^{i\omega t}, \tag{52}$$

$$\bar{w}(x,t) = [\bar{F}_1\bar{a}e^{-i\bar{k}_1 x} + \bar{F}_2\bar{b}e^{-i\bar{k}_2 x} - \bar{F}_1\bar{c}e^{i\bar{k}_1 x} - \bar{F}_2\bar{d}e^{i\bar{k}_2 x}]\, e^{i\omega t}. \tag{53}$$

For the region $x \geqslant D$ the deformation is given by

$$\theta_L(x,t) = [a_t e^{-ik_1 x} + b_t e^{-ik_2 x}]e^{i\omega t}, \tag{54}$$

$$w_L(x,t) = [a_t F_1 e^{-ik_1 x} + b_t F_2 e^{-ik_2 x}]e^{i\omega t}. \tag{55}$$

There are a total of 10 unknowns $(a_r, b_r, \bar{a}, \bar{b}, \bar{c}, \bar{d}, \bar{g}, \bar{h}, a_t, b_t)$ which can be determined from the following continuity and equilibrium conditions:

$$\theta_- = \bar{\theta}, \quad w_- = \bar{w}, \quad \bar{u} = -\theta_-\frac{h}{4}, \quad V_- = 2\bar{V}, \quad M_- = 2\bar{M} - 2\bar{T}\frac{h}{4} \quad (\text{at } x = 0), \tag{56a}$$

$$\theta_L = \bar{\theta}, \quad w_L = \bar{w}, \quad u_L = -\theta_-\frac{h}{4}, \quad V_L = 2\bar{V}, \quad M_L = 2\bar{M} - 2\bar{T}\frac{h}{4} \quad (\text{at } = l). \tag{56b}$$

Numerical results of the reflection and transmission ratios, defined by Eqs. (22 and 23), are shown in Fig. 10 for three different ratios of delamination length to beam thickness. As opposed to the

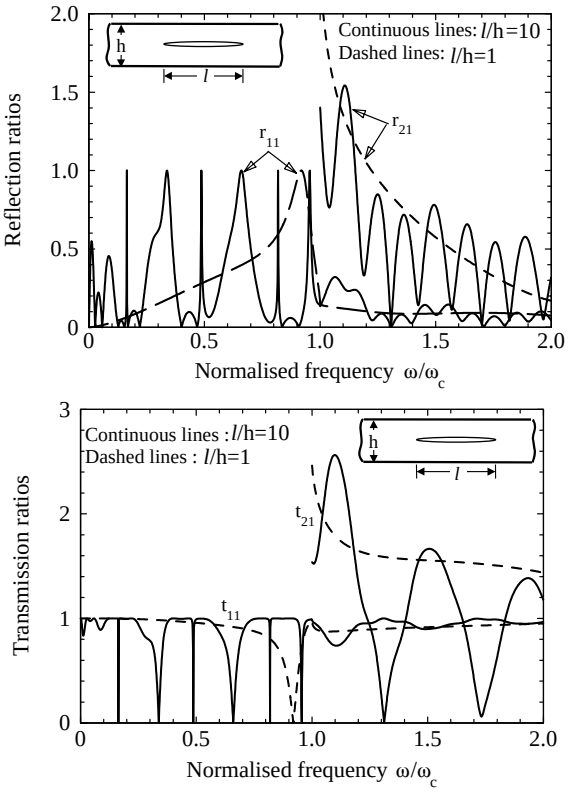

Fig. 10. Influence of a symmetric delamination on wave reflection and transmission; (a) reflection oefficients and (b) transmission coefficients.

inhomogeneity approach, the micro-mechanics approach for mid-plane delamination produces a stronger pass/stop band behaviour, with the reflection ratio reaching unity at certain frequencies, which depends on the size of the delamination. An important implication of this pass/stop band behaviour is that the main detection frequency needs to be optimized to achieve the maximum sensitivity. This phenomenon is currently being exploited.

5. Comparison with experimental results

To demonstrate the potential of the present theoretical approach, a comparison is presented in the following between the theoretical predictions and the experimental results of Diaz Valdes and Soutis [6]. Their specimen, which was made of quasi-isotropic carbon epoxy laminate, is sketched in Fig. 11 showing the dimensions. From the elastic moduli of the unidirectional ply [6], Young's modulus of laminate along the beam length direction is determined to be 50.7 GPa. Other relevant properties are : shear modulus = 5.7 GPa and density = 1536 kg/m^3.

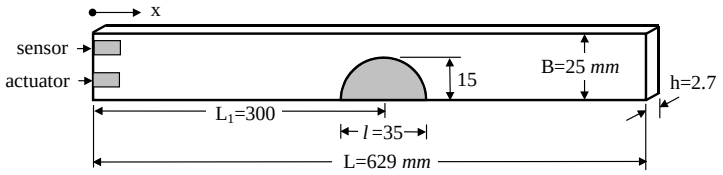

Fig. 11. Geometry and dimension of a beam specimen.

The actuator was excited by a 15 kHz sinusoidal pulse of 5.5 cycles modulated by a Hanning window. Thus, the input strain at $x=0$ due to this excitation can be mathematically described by

$$\varepsilon_e(t) = \begin{cases} -\varepsilon_0 \ \sin(2\pi f_0 t)\dfrac{1-\cos(2\pi f_0 t/5.5)}{2}, & 0 \leqslant t \leqslant 5.5/f_0, \\ 0, & \text{otherwise}, \end{cases} \tag{57}$$

where $f_0 = 15\,\text{kHz}$. Since the actuator was attached at one free end of the beam, only flexural wave was excited; similarly only the flexural component of the reflected wave was recorded by the sensor located next to the actuator. The response at the sensor location $x=0$ comprises the reflection from the delamination region, and the wave packet that has travelled the round trip (transmitted across the delamination, reflected off the other free end of beam, and then re-transmitted through the delamination). Due to the relatively low frequency being employed (excitation frequency is only 5% the cut-off frequency of the second flexural wave), it suffices to consider only the first mode of flexural wave, consequently the Fourier transform of the response at the sensor location is given by

$$\int_{-\infty}^{\infty} \varepsilon(t)\mathrm{e}^{\mathrm{i}\omega t}\,\mathrm{d}t = (1 + r_{11}\mathrm{e}^{-2\mathrm{i}k_1(L_1-l/2)} - t_{11}^2\mathrm{e}^{-2\mathrm{i}k_1 L}) \int_{-\infty}^{\infty} \varepsilon_e(t)\mathrm{e}^{\mathrm{i}\omega t}\,\mathrm{d}t, \tag{58}$$

where the reflection ratio r_{11} and the transmission ratio t_{11}, both being frequency dependent, are determined from the method presented in Sections 3 and 4 for the homogenization approach and the split beam approach, respectively. The second term inside the bracket represents the reflection from the delamination, whereas the third term represents the signal that travelled the "round-trip": first traversing through the delamination, being reflected from the free end, and then traversing through the delamination before reaching the sensor. The minus sign in front of the transmission ratio t_{11} is to account for the reflection at the free end. Here the reflection ratio r_{11} and the transmission ratio t_{11} represents the phase discontinuities produced by the multiple reflection and transmission process. Responses in the absence of damage can be readily recovered by setting $r_{11} = 0$ and $t_{11} = 1$. The forward and inverse Fourier transform can be performed by the fast Fourier transform technique [27].

Since the actual delamination employed by Diaz Valdes and Soutis [6] was part through the width of the beam, it is necessary to approximate the delamination by an equivalent through-width delamination that has the same area as the actual delamination. Denoting the damage of the delamination region as A_d, the length of the equivalent damage size l_{eq} is given by

$$l_{eq} = A_d/B, \tag{59}$$

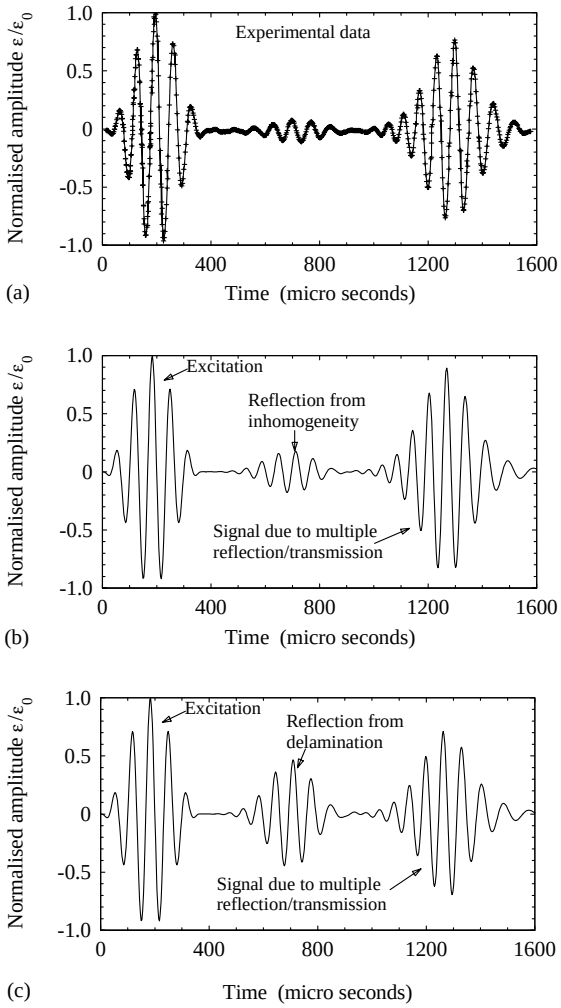

Fig. 12. Comparison between predictions and experimental data; (a) experimental results by Diaz Valdes and Soutis [6], (b) predictions of inhomogeneity approach, and (c) predictions of split-beam approach.

where B denotes the width of the specimen. For the largest delamination (area = 400 mm^2) being considered, this gives an equivalent damage size of $l_{eq} = 16$ mm. The predictions of the two methods, together with the experimental results are shown in Fig. 12. Here a time window of 3000 μs with 1024 sampling points are used in the forward and inverse fast Fourier transform, corresponding to a Nyquist frequency of 170 kHz, about 10 times the centre frequency of the excitation. It can be seen that the equivalent inhomogeneity approach yields a very good estimate of the reflected wave from the delamination, whereas the split beam method overpredicts the reflections. This discrepancy could be attributed to the fact the actual delamination is only partly through the width of the specimen, which restricts the relative motions between the delaminated layers. On the other hand, for the signal reflected from the far end of the beam, which has experienced twice transmission through the delamination region during the round trip, the

equivalent inhomogeneity approach overestimates the actual response, whereas the split beam method provides a better correlation with the measured data.

6. Conclusions

By employing higher order plate theories, analytical solutions have been obtained for the reflections from and transmissions through a damaged region in a beam. The damaged region can either be modelled as an inhomogeneity with a reduced bending rigidity, or as a split beam representing delamination. in both cases the plate theory approach allows the complex mode conversion and the infinite reflections and transmissions due to a finite size damage to be quantified analytically. However, an extension to 2-D wave scattering is much more readily achieved by the homogenization approach, as developed by Rose and Wang [18,19]. The favourable comparison of the present 1-D theory with experimental results is encouraging from the viewpoint of structural health monitoring.

Appendix A. Nomenclature

c_p	phase velocity ($=\omega/k$)
c_g	group velocity ($=\mathrm{d}\omega/\mathrm{d}k$)
c_0	rod wave speed ($=\sqrt{E/\rho(1-\nu^2)}$)
c_ℓ	longitudinal wave speed ($=c_s\sqrt{2(1-\nu)/(1-2\nu)}$)
c_s	shear velocity ($=\sqrt{G/\rho}$)
E	Young's modulus
E'	Young's modulus under plane-strain conditions ($=E/(1-\nu^2)$)
f	frequency
F	ratio between displacement and angle of rotation
G	shear modulus
h	thickness
I	flexural stiffness
k	wave number
l	size of damage
M	bending moment
P	power carried by propagating waves
q	radius of gyration ($=\sqrt{I/A}$)
r	reflection coefficient
t	transmission coefficient
T	longitudinal force
u	longitudinal displacement
V	shear force
w	transverse displacement

Greek symbols

κ	shear correction factor ($= \pi/\sqrt{12}$)
λ	wavelength ($= 2\pi/k$)
ρ	density
ω	angular frequency ($= 2\pi/f$)
ω_c	cut-off frequency of the second flexural mode ($= \pi c_s/h$)
ω_{ce}	cut-off frequency of the second extensional mode ($= \pi c_\ell/h$)
v	the Poisson's ratio
θ	angle of rotation

Superscript

$*$	damaged region

Subscripts

ℓ	longitudinal waves
r	reflected waves
t	transmitted waves

References

[1] F.-K. Chang, Smart-layer: built-in diagnostics for composite structures, Proceedings of the Fourth European Conference on Smart Structures and Materials, IOPP, Bristol, UK, 1998.

[2] C. Boller, Fundamentals on damage monitoring, in: Smart Structures and Materials: Implications for Military Aircraft of New Generation, AGARD SMP Lecture Series, LS-205, 1996.

[3] C. Boller, Ways and options for aircraft structural health management, Smart Materials and Structures 10 (2001) 432–440.

[4] N. Guo, P. Cawley, Lamb wave reflection for the quick nondestructive evaluation of large composite laminates, Material Evaluations 52 (1994) 404–411.

[5] A. Birt, Damage detection in carbon-fibre composites using ultrasonic Lamb waves, Insight 40 (1998) 335–339.

[6] S.H. Diaz Valdes, C. Soutis, Health monitoring of composites using Lamb waves generated by piezoelectric devices, Plastics, Rubber and Composites 29 (2000) 475–481.

[7] N. Rajic, In situ monitoring of crack growth in mild steel under closure conditions using a piezotransducer array, Journal of Intelligent Materials and Structures 11 (2000) 696–702.

[8] E.V. Malyarenko, M.K. Hinders, Fan beam and double crosshole Lamb wave tomography for mapping flaws in aging aircraft structures, Journal of the Acoustical Society America 108 (2000) 1631–1639.

[9] M. Lemistre, D. Balageas, Structural health monitoring system based on diffracted Lamb wave analysis by multiresolution processing, Smart Materials and Structures 10 (2001) 504–511.

[10] S.V. Kulkarni, D. Frederick, Frequency as a parameter in a delamination problem—a preliminary investigation, Journal of Composite Materials 5 (1971) 112–119.

[11] J.J. Tracy, G.C. Pardoen, Effect of delamination on the natural frequencies of composite laminates, Journal of Composite Materials 23 (1989) 1200–1215.

[12] S.H. Diaz Valdes, C. Soutis, Delamination detection in composite laminates from vibrations of their modal characteristics, Journal of Sound and Vibration 228 (1999) 1–9.

[13] A. Vary, Acousto-ultrasonics: retrospective exhortation with bibliography, Material Evaluation 49 (1991) 581–591.

[14] I.A. Viktorov, Rayleigh and Lamb Waves, Plenum Press, New York, 1967.
[15] T.C. Bache, G.A. Hegemier, On higher-order elastodynamic plate theories, Journal of Applied Mechanics 31 (1974) 423–428.
[16] R.D. Mindlin, Influence of rotatory inertia and shear on flexural motions of isotropic, elastic plates, Journal of Applied Mechanics 18 (1951) 31–38.
[17] T.R. Kane, R.D. Mindlin, High-frequency extensional vibrations of plates, Journal of Applied Mechanics 23 (1956) 277–283.
[18] L.R.F. Rose, C.H. Wang, Mindlin plate theory for damage detection II. Scattering by flexural inhomogeneities, Journal of Acoustical Society America, submitted for publication.
[19] L.R.F. Rose, C.H. Wang, Mindlin plate theory for damage detection III. Part-through, through cracks, Journal of the Acoustical Society America, submitted for publication.
[20] M.R. Gorman, W.H. Prosser, Application of normal mode expansion to acoustic emission waves in finite plates, Journal of Applied Mechanics 63 (1996) 555–557.
[21] J.F. Doyle, S. Kamle, An experimental study of the reflection and transmission of flexural waves at discontinuities, Journal of Applied Mechanics 52 (1985) 669–673.
[22] J.T.S. Wang, Y.Y. Liu, J.A. Gibby, Vibrations of split beams, Journal of Sound and Vibration 84 (1982) 491–502.
[23] P.M. Mujumdar, S. Suryanarayan, Flexural vibrations of beams with delaminations, Journal of Sound and Vibration 125 (1988) 441–461.
[24] T.N. Farris, J.F. Doyle, Wave propagation in split Timoshenko, Journal of Sound and Vibration 130 (1989) 137–147.
[25] B.R. Mace, R.W. Jones, N.R. Harland, Wave transmission through structural inserts, Journal of the Acoustical Society America 109, 1417–1421.
[26] Y.-Y Yu, Vibrations of Elastic Plates, Springer, New York, 1995.
[27] J.F. Doyle, Wave Propagation in Structures, 2nd Edition, Springer, New York, 1997.
[28] B.R. Mace, Wave reflection and transmission in beams, Journal of Sound and Vibration 97 (1984) 237–246.
[29] L. Cremer, M. Heckl, Structure-Borne Sound, 2nd Edition, Springer, Berlin, 1973.
[30] D.J. Mead, Passive Vibration Control, Wiley, Chichester, UK, 1998, p.157.